UNIVERSIDADE FEDERAL DO CEARÁ
CENTRO DE CIÊNCIAS
DEPARTAMENTO DE QUÍMICA ANALÍTICA E FÍSICO-QUÍMICA
PROGRAMA DE PÓS-GRADUAÇÃO EM QUÍMICA

JOSÉ OSMAR DE SOUZA JÚNIOR

STUDY OF Sn^{2+} AND In^{3+} IONS IN THE DEEP EUTECTIC SOLVENT ETHALINE WITH SURFACTANTS: ANALYSIS OF INTERACTIONS THROUGH MOLECULAR DYNAMICS, QUANTUM THEORY OF ATOMS IN MOLECULES AND ELECTRON LOCALIZATION FUNCTION

FORTALEZA
2024

JOSÉ OSMAR DE SOUZA JÚNIOR

STUDY OF Sn^{2+} AND In^{3+} IONS IN THE DEEP EUTECTIC SOLVENT ETHALINE WITH SURFACTANTS: ANALYSIS OF INTERACTIONS THROUGH MOLECULAR DYNAMICS, QUANTUM THEORY OF ATOMS IN MOLECULES AND ELECTRON LOCALIZATION FUNCTION

Dissertação apresentada ao Programa de Pós-Graduação em Química da Universidade Federal do Ceará, como requisito parcial à obtenção do título de Mestre em Química. Área de concentração: Físico-Química.

Orientador: Prof. Dr. Norberto de Kássio Vieira Monteiro.

FORTALEZA

2024

Dados Internacionais de Catalogação na Publicação
Universidade Federal do Ceará
Sistema de Bibliotecas
Gerada automaticamente pelo módulo Catalog, mediante os dados fornecidos pelo(a) autor(a)

S238s Souza Júnior, José Osmar de.
Study of Sn2+ and In3+ ions in the Deep Eutectic Solvent ethaline with surfactants: analysis of interactions through Molecular Dynamics, Quantum Theory of Atoms in Molecules and Electron Localization Function / José Osmar de Souza Júnior. – 2024.
49 f. : il. color.

Dissertação (mestrado) – Universidade Federal do Ceará, Centro de Ciências, Programa de Pós-Graduação em Química, Fortaleza, 2024.
Orientação: Prof. Dr. Norberto de Kássio Vieira Monteiro.
Coorientação: Profa. Dra. Adriana Nunes Correia.

1. Electrodeposition. 2. Ethaline. 3. Tin and Indium. 4. CTAB. 5. SDS. I. Título.
CDD 540

JOSÉ OSMAR DE SOUZA JÚNIOR

STUDY OF Sn^{2+} AND In^{3+} IONS IN THE DEEP EUTECTIC SOLVENT ETHALINE WITH SURFACTANTS: ANALYSIS OF INTERACTIONS THROUGH MOLECULAR DYNAMICS, QUANTUM THEORY OF ATOMS IN MOLECULES AND ELECTRON LOCALIZATION FUNCTION

Dissertação apresentada ao Programa de Pós-Graduação em Química da Universidade Federal do Ceará, como requisito parcial à obtenção do título de Mestre em Química. Área de concentração: Físico-Química.

Aprovada em: 30/08/2024.

BANCA EXAMINADORA

_____

Prof. Dr. Norberto de Kássio Vieira Monteiro (Orientador)
Universidade Federal do Ceará (UFC)

_____

Profa. Dra. Adriana Nunes Correia (Coorientadora)
Universidade Federal do Ceará (UFC)

_____

Prof. Dr. Paulo Naftali da Silva Casciano
Universidade Federal do Ceará (UFC)

To my parents, Verônica and Osmar.

ACKNOWLEDGMENTS

To my parents, Geralda Verônica Saraiva Silva and José Osmar de Souza, and to my aunt, Margarida Deusa Saraiva Silva, for all the love and education that were shared with me over the years.

To all my relatives who have contributed directly or indirectly to my integral formation.

To my cousin, Gisele Saraiva da Cunha, my safe haven, for being there to listen when I needed it most.

To my friends, members and former members of the Grupo de Química Teórica (2022 - 2024), for the experiences and good moments shared during the master's years: Renato Veríssimo de Oliveira, Lucas Pinheiro Coutinho, Lucas Lima Bezerra, Leonardo Paes da Silva, Gizele do Nascimento de Castro, José de Nazareno Ferreira dos Santos, Marcus Vinícius Fernandes Rodrigues, Denilson Silvino da Silva, Diego do Nascimento Gomes, José Marques Neto, and Laudenor Amorim.

To my apodictic friends, Renato Veríssimo de Oliveira and Lucas Pinheiro Coutinho: your experiences and privileged way of understanding the world inspire me to make the pursuit of knowledge my life's mission.

To Prof. Dr. Norberto de Kássio Vieira Monteiro, Profa. Dra. Adriana Nunes Correia, Prof. Dr. Paulo Naftali da Silva Casciano and Prof. Dr. Pedro de Lima Neto. Especially to my advisor, Prof. Dr. Norberto de Kássio Vieira Monteiro, for the excellent guidance and suggestions that allowed the concretization of this work.

To the Universidade Federal do Ceará, for the space and all the opportunities offered in the last years.

To the Centro Nacional de Processamento de Alto Desempenho (CENAPAD) of the Universidade Federal do Ceará (UFC) and Universidade Estadual de Campinas (UNICAMP) for the computational resources offered.

To CAPES for the finantial support. This study was financed in part by the Coordenação de Aperfeiçoamento de Pessoal de Nível Superior – Brasil (CAPES) – Finance Code 001.

“The most that can be expected from any model is that it can supply a useful approximation to reality. All models are wrong; some models are useful.” (George E. P. Box, William Hunter and Stuart Hunter, 2005, p. 440).

RESUMO

Este trabalho utiliza métodos computacionais para investigar o comportamento dos íons Sn^{2+} e In^{3+} no DES etalina sob diferentes condições. A Teoria do Funcional da Densidade (DFT) foi aplicada para otimização, e o método CHELPG foi utilizado para atribuição de cargas parciais. Foram realizadas doze simulações de Dinâmica Molecular (MD), utilizando o software GROMACS, em diferentes temperaturas (297 K e 343 K), proporções de íons [Sn:In (1:1 e 1:4)], e na presença e ausência de diferentes surfactantes (CTAB e SDS). Adicionalmente, as propriedades oriundas da Teoria Quântica de Átomos em Moléculas (QTAIM) foram obtidas após simulações MD. Os resultados mostraram que o In^{3+} apresentou uma maior afinidade com o Cl^- do que o Sn^{2+}, mas interações mais fracas e menos estáveis com o OA (OA = oxigênio do etilenoglicol), particularmente a temperaturas mais elevadas. As análises da densidade eletrônica e da função de localização de eletrônica indicaram que as interações In-Cl são mais fortes e mais polarizadas do que as demais interações. O laplaciano da densidade eletrônica indicou uma natureza intermolecular para todas as interações. Os gráficos moleculares mostraram uma geometria octaédrica em torno do Sn^{2+} e uma geometria tetraédrica ou bipirâmide trigonal em torno do In^{3+}. A adição de tensoativos alterou ligeiramente essas interações, com o CTAB reduzindo a densidade de Cl^- em torno do In^{3+} e o SDS interagindo com o In^{3+} a 297 K e em uma proporção Sn:In de 1:1.

Keywords: eletrodeposição; etalina; estanho e índio; CTAB; SDS.

ABSTRACT

This work uses computational methods to investigate the behavior of Sn^{2+} and In^{3+} ions in the DES ethaline under different conditions. The Density Functional Theory (DFT) was applied for optimization, and the CHELPG method was used for partial charges attribution. Twelve Molecular Dynamics (MD) simulations were conducted, using the GROMACS software, in different temperatures (297 K and 343 K), ion proportions [Sn:In (1:1 and 1:4)], and in the presence and absence of different surfactants (CTAB and SDS). Additionally, Quantum Theory of Atoms in Molecules (QTAIM) properties were obtained after MD simulations. The results presented that In^{3+} showed stronger affinity for Cl^{-} than Sn^{2+}, but weaker and less stable interactions with OA (OA = oxygen of ethylene glycol), particularly at higher temperatures. Electron Density and Electron Localization Function analysis indicated that In-Cl interactions are stronger and more polarized than other interactions. The laplacian of electron density suggested an intermolecular nature for all interactions. The molecular graphs showed octahedral geometry around Sn^{2+} and tetrahedral or trigonal bipyramidal geometry around In^{3+}. The surfactant addition altered these interactions slightly, with CTAB reducing the density of Cl^{-} around In^{3+} and SDS interacting with In^{3+} at 297 K and in a Sn:In proportion of 1:1.

Keywords: electrodeposition; ethaline; tin and indium; CTAB; SDS.

LIST OF FIGURES

LIST OF TABLES

LIST OF ABBREVIATIONS AND ACRONYMS

B3LYP	Becke-3-Parameter-Lee-Yang-Parr
BCP	Bond Critical Point
CCN	Cumulative Coordination Number
CHELPG	CHarges from ELectrostatic Potentials using a Grid-based method
ChCl	Choline Chloride
CTAB	Cetyltrimethylammonium Bromide
DES	Deep Eutectic Solvents
DFT	Density Functional Theory
EG	Ethylene glycol
ELF	Electron Localization Function
GROMACS	GROningen MAchine for Chemical Simulations
LANL2DZ	Los Alamos National Laboratory 2-double-z
M06-2X	Minnesota Functionals, 06 family
MD	Molecular Dynamics
NPT	Isothermal-Isobaric ensemble
NVT	Canonical ensemble
OPLS-AA	Optimized Potentials for Liquid Simulations - All Atom
QTAIM	Quantum Theory of Atoms in Molecules
RDF	Radial Distribution Function
SDS	Sodium Dodecyl Sulfate

SUMMARY

1. Introduction

Sn-based solders share common characteristics of low melting point [1-3] and ductility [3]. The insertion of other metals, like In, into alloys containing Sn changes the properties of the weld, such as hardness and stability. [4] Few published works address using Sn-In alloys in deep eutectic solvents (DES). [5-7] Anicai *et al*. [5] studied the electrodeposition of SnIn in ethaline [choline chloride/ethylene glycol 1:2 (1ChCl:2EG)] medium. As a result of the investigations, the authors verified that the In content increased due to the change in the Sn^{2+}: In^{3+} ionic species' molar ratio and the temperature increase. The results obtained showed good performance regarding weldability and corrosion resistance.

Oliveira *et al*. [6] analyzed the ionic interaction of Sn^{2+} and In^{3+} ions in ethaline by molecular modeling. The results indicated that both ions interacted more strongly with the Cl^- ion. However, only the Sn^{2+} ion showed interaction with the ethylene glycol molecules. Sousa *et al.* [7] analyzed the effect of temperature and potential on the electrodeposition of SnIn in ethaline medium with $InCl_3$ and $SnCl_2$ as the source of cations and with simulations using Molecular Dynamics (MD) [8]. Scanning electron microscopy (SEM) images showed morphologies for different coatings under the influence of temperature and applied potential. Analysis by energy dispersive X-rays (EDS) resulted in In content between 20-31% in equimolar conditions of Sn^{2+} and In^{3+}. The results of MD simulations for Sn^{2+} and In^{3+} ions in DES showed similarity with Oliveira *et al.* [6], justifying the low percentage of In obtained.

The use of additives can influence the properties of the coatings obtained. Among the additives, we can mention surfactants, which can change the morphology, [9,10] corrosion resistance, [11,12] purity of the coating, [13] surface tension of the solution, [13] etc. Electrodeposition using surfactants has been investigated for some metals, such as Ag, using the surfactants hexadecyltrimethylammonium bromide (CTAB) and sodium dodecyl sulfate (SDS) [14]; Zn, using SDS and polyacrylic acid [15]; MnO_2, using benzyl dodecyl dimethylammonium bromide (B-AB) [16], etc.

MD simulations present potential for evaluating the influence of surfactants in electrodeposition processes. Wickramaarachchi *et al.* [16] studied, using MD, how the surfactant B-AB affects electrodeposition by adsorbing on the lead surface and influencing the nucleation and growth of MnO_2 deposits. The results showed that B-AB improved the electrochemical properties of MnO_2 by adsorption on Pb surfaces. The surfactant

concentration affected the aggregate formation and surface saturation. Additionally, according to Aribou *et al.* [17], MD was used to elucidate the mechanism of electrodeposition of copper in the presence of the additive ANP [poly(oxy-1,2-ethanediyl), alpha-(4-nonylphenyl)-omega-hydroxy-,branched], allowing to understand how ANP is adsorbed on the surfaces of brass and copper and how it affects the morphology of the electrodeposits of copper. The simulations showed that ANP molecules adsorb more strongly on copper surfaces than on zinc, as indicated by the adsorption energies −108.46 kcal mol^{-1} and −33.54 kcal mol^{-1} for Cu (111) and Zn (111), respectively.

Based on the influence of surfactants and molecular modeling potential insights, it's essential to explore the behavior of chemical species in solution to evaluate the relation between the interactions in solution and electrodeposition. The objective of the present work was to theoretically analyze the effect of adding CTAB and SDS to ethaline using $InCl_3$ and $SnCl_2$. In the computer simulation studies, the techniques of Molecular Dynamics (MD) and Quantum Theory of Atoms in Molecules (QTAIM) [18] were used, as they are essential to microscopically understand the behavior of interactions between the components of the system.

2. Theoretical Foundation

The methods of theoretical chemistry and molecular modeling can be classified into three main approaches: empirical, quantum, and hybrid methods [19]. In this work, one empirical method - the Molecular Dynamics (MD) -, and two quantum methods - the Density Functional Theory (DFT) and the Quantum Theory of Atoms in Molecules (QTAIM) - have been used. The following subtopics present theoretical details of MD and QTAIM methods, which are the primary focus of the results.

2.1. Molecular Dynamics (MD)

Molecular Dynamics is based the Molecular Mechanics, in which each atom in a chemical system is treated as a point to which a mass is attributed, while the interactions are treated as "springs". The movement of particles is based on Newton's second law:

$$F_i(t) = m_i a_i \quad (1)$$

where m_i is the mass of the particle, a_i is the acceleration, and F_i represents the sum of the forces acting on a determined particle [8].

The forces exerted in each atom are calculated from the negative gradient of the potential energy as a function of the atomic positions:

$$F_i(t) = -\nabla U(r_1, r_2, \ldots, r_N) \quad (2)$$

where U is the potential energy function and r_N is the position vector of the atom i (i = 1, 2, ..., N) [20]. The Force Field, a very common term in this context, is considered an expression of the potential energy, and its choice depends on the chemical system being studied and of the level of accuracy required. The main components of the potential energy are given in the relation below:

$$U = U_L + U_\theta + U_\omega + U_{NL} \quad (3)$$

where U_L is the potential energy associated with the stretching of the bonds; U_θ with the distortion of the plane angles; U_ω with the distortion of the dihedral angles; U_{NL} with the non-bonded interactions, these being divided into electrostatic (coulombic) interactions and Van der Waals interactions [21].

2.1.1. Integration methods

In MD simulations, the integration of the movement equation is performed by numerical methods, such as the Verlet and Leapfrog algorithms, with the objective of determining the trajectory of the atoms of the system over time.

In the Verlet algorithm [22], the positions of the particles are updated according to the equation below:

$$r(t + \Delta t) = 2r(t) - r(t - \Delta t) + a(t)\Delta t^2 \quad (4)$$

where $r(t)$ represents the position of a particle in the time t; Δt is the time interval; and $a(t)$ is the acceleration of the particle in the time t. The acceleration, $a(t)$, is calculated by dividing the sum of the forces acting on the particle by its mass, in accordance with Newton's second Law, $a(t) = \frac{F(t)}{m}$.

The operation of the Verlet algorithm can be described in terms of a series of steps, which are constituted by sequential iterations performed by a loop. It is important to note that the description that will be presented is an example, which is intended to facilitate the visualization of how the algorithm works. A similar approach will be taken in relation to the Leapfrog algorithm.

In the first iteration, in which t = 0, there are initial attributions for the initial position of the particles [$r(0)$], and for the position in a time interval preceding the initial time [$r(-\Delta t)$]. The initial acceleration, $a(0)$, can be calculated from the initial forces, in $F(0)$. Considering these attributions, we obtain the position of the particles in $r(\Delta t)$, as presented in the following expression:

$$r(\Delta t) = 2r(0) - r(-\Delta t) + a(0)\Delta t^2 \quad (5)$$

In the second iteration, in which $t = \Delta t$, new attributions are introduced. The first term of the second member of the equation (4) becomes the double of the position of the particle in the time interval Δt [$2r(\Delta t)$], that is, the double of the value for the position obtained in the previous iteration. The second term of the second member becomes $r(0)$. Finally, the new acceleration is calculated in the time interval Δt [$a(\Delta t)$]. Consequently, the equation of the second iteration is as follows:

$$r(2\Delta t) = 2r(\Delta t) - r(0) + a(\Delta t)\Delta t^2 \quad (6)$$

For the third iteration:

$$r(3\Delta t) = 2r(2\Delta t) - r(\Delta t) + a(2\Delta t)\Delta t^2 \quad (7)$$

So, for the n[th] iteration, we have:

$$r(n\Delta t) = 2r((n-1)\Delta t) - r((n-2)\Delta t) + a((n-1)\Delta t)\Delta t^2 \quad (8)$$

This procedure will be repeated in accordance with the predefined parameters prior to the execution of the production step of the MD simulation, which is conducted using appropriate software, such as GROMACS.

The Leapfrog algorithm represents the integration method employed in this work. In contrast to the Verlet method, in which the velocity is a non-binding variable, it is a necessary component in the Leapfrog algorithm. In this algorithm, the update of velocity is used for the update in position. From the definition of acceleration and assuming an increment time equal to $\frac{\Delta t}{2}$, it is possible to apply a central finite differentiation [23] in t, in accordance with the following expression:

$$a(t) \approx \frac{v\left(t + \frac{\Delta t}{2}\right) - v\left(t - \frac{\Delta t}{2}\right)}{\Delta t} \quad (9)$$

It can be rearranged to obtain the equation of the velocity update of particles:

$$v\left(t + \frac{\Delta t}{2}\right) = v\left(t - \frac{\Delta t}{2}\right) + a(t)\Delta t \quad (10)$$

In order to obtain the expression related to the position update, it is necessary to begin with the definition of velocity. Once again, an increment time equal to $\frac{\Delta t}{2}$ must be considered, and a central finite differentiation must be applied in $t + \frac{\Delta t}{2}$, in accordance with the following equation:

$$v\left(t + \frac{\Delta t}{2}\right) \approx \frac{r(t + \Delta t) - r(t)}{\Delta t} \quad (11)$$

It can be rearranged to obtain the equation of the position update of particles:

$$r(t + \Delta t) = r(t) + v\left(t + \frac{\Delta t}{2}\right)\Delta t \quad (12)$$

The equations (10) and (12) represent the principal relations that underlie the Leapfrog algorithm [24].

Finally, as the running of the algorithm also corresponds to a sequence of iterations within a loop, it can be demonstrated that, for the first iteration, at t = 0, the values attributed

will be $v\left(-\frac{\Delta t}{2}\right)$ and $a(0)\Delta t$. This results in a new velocity being equal to $v\left(\frac{\Delta t}{2}\right)$. The updated value for velocity is then used to obtain the updated position. The input values for the position expression are $r(0)$ and $v\left(\frac{\Delta t}{2}\right)\Delta t$, which are used to obtain $r(\Delta t)$. The expressions for updates in velocity and position for the first iteration are as follows:

$$v\left(\frac{\Delta t}{2}\right) = v\left(-\frac{\Delta t}{2}\right) + a(0)\Delta t$$

$$r(\Delta t) = r(0) + v\left(\frac{\Delta t}{2}\right)\Delta t \tag{13}$$

In accordance with the logic employed in the first algorithm presented, for the second iteration, in which $t = \Delta t$, the following expressions for updates in velocity can be obtained:

$$v\left(\frac{3\Delta t}{2}\right) = v\left(\frac{\Delta t}{2}\right) + a(\Delta t)\Delta t$$

$$r(2\Delta t) = r(\Delta t) + v\left(\frac{3\Delta t}{2}\right)\Delta t \tag{14}$$

In the third iteration, the expressions below are obtained:

$$v\left(\frac{5\Delta t}{2}\right) = v\left(\frac{3\Delta t}{2}\right) + a(2\Delta t)\Delta t$$

$$r(3\Delta t) = r(2\Delta t) + v\left(\frac{5\Delta t}{2}\right)\Delta t \tag{15}$$

Given the observed trend, for the n[th] iteration, where $t = (n-1)\Delta t$, the following can be concluded:

$$v\left(\left(n - \frac{1}{2}\right)\Delta t\right) = v\left(\left(n - \frac{3}{2}\right)\Delta t\right) + a((n-1)\Delta t)\Delta t$$

$$r(n\Delta t) = r((n-1)\Delta t) + v\left(\left(n - \frac{1}{2}\right)\Delta t\right)\Delta t \tag{16}$$

For illustrative purposes of a MD running, the equations (8) and (16) represent generalizations that could be employed in a code or pseudocode, particularly in a control structure or loop, given that both Verlet and Leapfrog methods are looping algorithms [25, 26]. The variable representing the termination condition is the number of iterations, which is incorporated into the equations of the Leapfrog algorithm.

2.1.2. Radial Distribution Function [g(r)] e Cumulative Coordination Number (CCN)

The Radial Distribution Function [$g(r)$], is a method that can be used to quantify the interactions between the particles in a system. This function provides information related to the probability of finding a particle at a distance r from a reference particle. It can be described as follows [27]:

$$g_{\alpha\beta}(r) = \frac{\rho_{\alpha\beta}(r)}{\rho_{\beta}} \tag{17}$$

where $\rho(r)$ is the local density of a particle β in a distance r from a reference particle α, and ρ_{β} is the average numerical density of the particle β in the system. In this work, the analysis of the chemical species that interact with the reference species was conducted in terms of Radial Distribution Function multiplied by the average numerical density [$g_{\alpha\beta}(r)\rho_{\beta}$]. Therefore, the graphs of $g(r)\rho\ x\ r$ can be interpreted as the local density of each species in function of the distance from the reference species.

The Cumulative Coordination Number (CCN) is the measure of the average cumulated quantity of particles in function of the distance. The equation for CCN, in accordance with [22], is given by:

$$N_{\alpha\beta}(r) = 4\pi\rho_{\beta}\int_{0}^{r} r^2\, g_{\alpha\beta}(r)dr \tag{18}$$

Applying a differentiation to the equation (18), the following result is obtained:

$$dN_{\alpha\beta}(r) = 4\pi\rho_{\beta}r^2 g_{\alpha\beta}(r)dr \tag{19}$$

Isolating $g_{\alpha\beta}(r)\rho_{\beta}$:

$$g_{\alpha\beta}(r)\rho_{\beta} = \frac{dN_{\alpha\beta}(r)}{4\pi r^2 dr} \tag{20}$$

Given that $4\pi r^2 dr = dV$, it can be concluded that:

$$g_{\alpha\beta}(r)\rho_{\beta} = \frac{dN_{\alpha\beta}(r)}{dV(r)} \tag{21}$$

Therefore, it can be observed that the CCN values are derived from the integration of the $g(r)$ function. Furthermore, the local density, $g(r)\rho$, can be understood as the rate of variation of the quantity of counter-species in relation to the differential volume element $dV(r)$ at a distance r from a reference species.

2.2. Topological properties

The Quantum Theory of Atoms in Molecules (QTAIM) is a theoretical model employed to investigate chemical bonds as well as to characterize intra- and intermolecular interactions. According to the principles of QTAIM, all the observable properties of a chemical system are contained in its electron density [ρ(r)]. Consequently, ρ(r) serves as a quantum-mechanical observable, being employed to calculate numeric integrals. In this context, the gradient vector, $\nabla\rho(r)$, is of fundamental importance in determining the molecular topology [28].

The electron density can present minimum or maximum regions, or saddle points, which are known as Critical Points (CPs). In this study, the topological properties – electron density [ρ(r)], laplacian of electron density [$\nabla^2\rho(r)$] and electron localization function [η(r)] – were obtained in regions designated as Bond Critical Points (BCPs). These are specific points that connect two attractors. The equation for the electron density is given by:

$$\rho(r) = \sum_i \eta_i |\varphi_i(r)|^2 = \sum_i \eta_i \left| \sum_\mu C_{\mu,i}\, \chi_\mu(r) \right|^2 \tag{22}$$

where φ is the orbital wavefunction, η is the occupation number, χ is the basis function and C is the coefficient matrix [29]. In the context of this work, the $\rho(r)$ numerical values can be understood as a measure of the strength of a chemical interaction.

The laplacian of electron density is given by:

$$\nabla^2\rho(r) = \frac{\partial^2\rho(r)}{\partial x^2} + \frac{\partial^2\rho(r)}{\partial y^2} + \frac{\partial^2\rho(r)}{\partial z^2} \tag{23}$$

The sign of numerical value of $\nabla^2\rho(r)$ characterizes the nature of a chemical interaction. Positive values indicate an intramolecular interaction, while negative values indicate an intermolecular interaction.

Finally, the expression for Electron Localization Function is presented below:

$$ELF(r) = \frac{1}{1 + \left(\frac{D(r)}{D_o(r)}\right)^2} \tag{24}$$

where $D(r)$ is the excess kinetic energy density caused by Pauli repulsion, while $D_o(r)$ is the Thomas-Fermi kinetic energy density, being considered a reference value. Likewise, the electron density, the $ELF(r)$, or η(r), is a measure of the strength of a chemical interaction,

once the larger the electron localization is in a region, once the greater the electron localization in a region, the higher the probability that electron motion is within it.

3. Objectives

3.1. General objective

To analyze, computationally, the behavior of the ions In^{3+} and Sn^{2+} in the deep eutectic solvent ethaline in the presence and absence of different surfactants (CTAB and SDS), at different temperatures (297 K and 343 K), and ion proportions[Sn:In (1:1 and 1:4)].

3.2. Specific objectives

- Investigate the main interactions between the reference ions and the counter-species using g(r)ρ;

- Determine the average quantity of counter-species around the reference ions using CCN;

- Evaluate the strength of the interactions using ρ(r) and ELF and the nature of the interactions using $\nabla^2\rho(r)$;

- Investigate the effect of surfactants in the interactions between the reference ions and the counter-species.

4. Methodology

4.1. Optimization of structures and obtaining partial charges

The optimization of ethylene glycol and choline components was conducted through the use of Density Functional Theory (DFT) [30-32] with the hybrid functional B3LYP [30, 33-35] and the basis set 6-311G+(d,p) in the GAUSSIAN 09 package [36]. Similarly, the surfactants, CTAB and SDS, were also optimized using the same hybrid functional, but with the basis set 6-31G+(d,p), once, for large structures, the use of a higher basis set is computationally demanding. The partial charges for all components were obtained through the CHELPG method [37] using Multiwfn 3.8 software [29].

4.2. Molecular dynamics (MD) simulation

A total of 12 MD simulations were performed for each specific system with the aim of evaluating the behavior of Sn^{2+} and In^{3+} ions in DES at two temperatures (297 K and 343 K), two proportions between the reference ions Sn:In (1:1 and 1:4), and in the absence and presence of different surfactants (CTAB, SDS), as shown in Table 1.

All MD simulations were performed using the GROMACS (GROningen MAchine for Chemical Simulations) 2020.4 software package [38]. The systems were simulated in twelve cubic boxes with dimensions of 12 nm × 12 nm × 12 nm, chosen as they were large enough to contain all the ions and molecules of the system. The simulated systems were characterized using the OPLS-AA [39] force field. The parameterization of SDS in the force field OPLS-AA was according to [40].

The quantities of each chemical species were determined aiming for the electroneutrality for each system, according to Table 1.

Table 1 Components and quantities used in each systems.

Temperature/K Proportion(Sn:In)	$Sn^{2+}In^{3+}$	$Sn^{2+}In^{3+}$ + CTAB	$Sn^{2+}In^{3+}$ + SDS
297 (1:1)	**Sn^{2+}:In^{3+} 1:1 (297 K)** Indium (26) Tin (26)	**Sn^{2+}:In^{3+} 1:1 + CTAB (297 K)** Indium (26) Tin (26)	**Sn^{2+}:In^{3+} 1:1 + SDS (297 K)** Indium (26) Tin (26)

	Choline (400) Ethylene glycol (800) Chloride (530)	Choline (400) Ethylene glycol (800) Chloride (530) Cetyltrimethylammonium (1) Bromide (1)	Choline (400) Ethylene glycol (800) Chloride (530) Sodium (8) Dodecyl sulfate (8)
297 (1:4)	**Sn^{2+}:In^{3+} 1:4 (297 K)** Indium (104) Tin (26) Choline (400) Ethylene glycol (800) Chloride (764)	**Sn^{2+}:In^{3+} 1:4 + CTAB (297 K)** Indium (104) Tin (26) Choline (400) Ethylene glycol (800) Chloride (764) Cetyltrimethylammonium (1) Bromide (1)	**Sn^{2+}:In^{3+} 1:4 + SDS (297 K)** Indium (104) Tin (26) Choline (400) Ethylene glycol (800) Chloride (764) Sodium (8) Dodecyl sulfate (8)
343 (1:1)	**Sn^{2+}:In^{3+} 1:1 (343 K)** Indium (26) Tin (26) Choline (400) Ethylene glycol (800) Chloride (530)	**Sn^{2+}:In^{3+} 1:1 + CTAB (343 K)** Indium (26) Tin (26) Choline (400) Ethylene glycol (800) Chloride (530) Cetyltrimethylammonium (1) Bromide (1)	**Sn^{2+}:In^{3+} 1:1 + SDS (343 K)** Indium (26) Tin (26) Choline (400) Ethylene glycol (800) Chloride (530) Sodium (8) Dodecyl sulfate (8)

343 (1:4)	**Sn^{2+}:In^{3+} 1:4 (343 K)** Indium (104) Tin (26) Choline (400) Ethylene glycol (800) Chloride (764)	**Sn^{2+}:In^{3+} 1:4 + CTAB (343 K)** Indium (104) Tin (26) Choline (400) Ethylene glycol (800) Chloride (764) Cetyltrimethylammonium (1) Bromide (1)	**Sn^{2+}:In^{3+} 1:4 + SDS (343 K)** Indium (104) Tin (26) Choline (400) Ethylene glycol (800) Chloride (764) Sodium (8) Dodecyl sulfate (8)

The energy minimizations of all systems, which aimed to optimize the geometry of the structures of the chemical species, were carried out using the steepest-descent algorithm [41] with an energy tolerance of 10.0 kJ mol^{-1} nm^{-1} and a total of 100000 steps, followed by the second minimization, carried out using the conjugate gradient method with an energy tolerance of 100.0 kJ mol^{-1} nm^{-1} and a total of 5000 steps. Subsequently, temperature equilibration was performed for 20 ns using the canonical ensemble (NVT) through Berendsen thermostat [42], followed by pressure equilibration, also performed for 20 ns using the isothermal-isobaric ensemble (NPT) through Parrinello-Rahman barostat [43]. Finally, the production stage of Molecular Dynamics was performed for 200 ns, using the same thermostat and barostat as the equilibration steps. The Lennard Jones parameters used to characterize the tin (Sn^{2+}) and indium (In^{3+}) ions were obtained from [44] and [28], respectively.

4.3. QTAIM topological properties

After the MD simulations, the equilibrium structures, derived from the production step, were employed as initial input for the QTAIM calculations executed by Multiwfn 3.8 software [29]. These calculations were conducted using the last frame from the production step obtained in the GROMACS software, applying 4.0 Å spherical cuts in all twelve systems. The metallic cations (Sn^{2+} and In^{3+}) were positioned at the origin (0, 0, 0) of the reference system solvated by adjacent species. Then, the derived systems were subjected to single-point calculations using the GAUSSIAN 09 package [36], with the M06-2X functional [45] and the

LANL2DZ basis set [46] for the Sn^{2+} and In^{3+} ions. On the other hand, the 6-31G+(d,p) basis set was utilized for the C, Cl, N, O, and H atoms. All topological data of electron density (ρ), Laplacian of electron density ($\nabla^2\rho$), and Electron Localization Function (ELF, η) were obtained using Multiwfn 3.8 software [29].

5. Results and Discussion

5.1. $Sn^{2+}In^{3+}$ 1:1 and $Sn^{2+}In^{3+}$ 1:4

The Radial Distribution Function multiplied by the average number density [g(r)ρ] serves to describe the density of a given counter-species at a distance "r" from a reference chemical species [47]. When comparing the $Sn^{2+}In^{3+}$ 1:1 systems, the following sequence of interactions is observed in descending order at 297 K: In-Cl > Sn-Cl > In-OA ≈ Sn-OA (OA = oxygen from ethylene glycol), where the counter-species are at a distance of approximately 2.0 Å, 3.0 Å, 1.8 Å, and 2.3 Å, respectively, as can be seen in Fig. 1a. The high density of chloride ions around In^{3+} can be attributed to the strength of In-Cl interaction, associated with the trivalence of indium, resulting in a strong electrostatic attraction with the chloride ions. Tin forms a bivalent cation, which contributes to the density of Cl^- being lower than around In^{3+} but still significant due to the electrostatic attraction. The lower density of OA around both ions is due to the nature of these interactions (ion-dipole). It can also be seen that the interactions with In^{3+} have a shorter length than those with Sn^{2+}. In addition to the contribution of the trivalent character, the ionic radius of indium, which is smaller, also influences the length of the interaction. According to Coulomb's Law, the electrostatic interaction strength is inversely proportional to the square of the distance, so the smaller the radius, the higher the interaction strength.

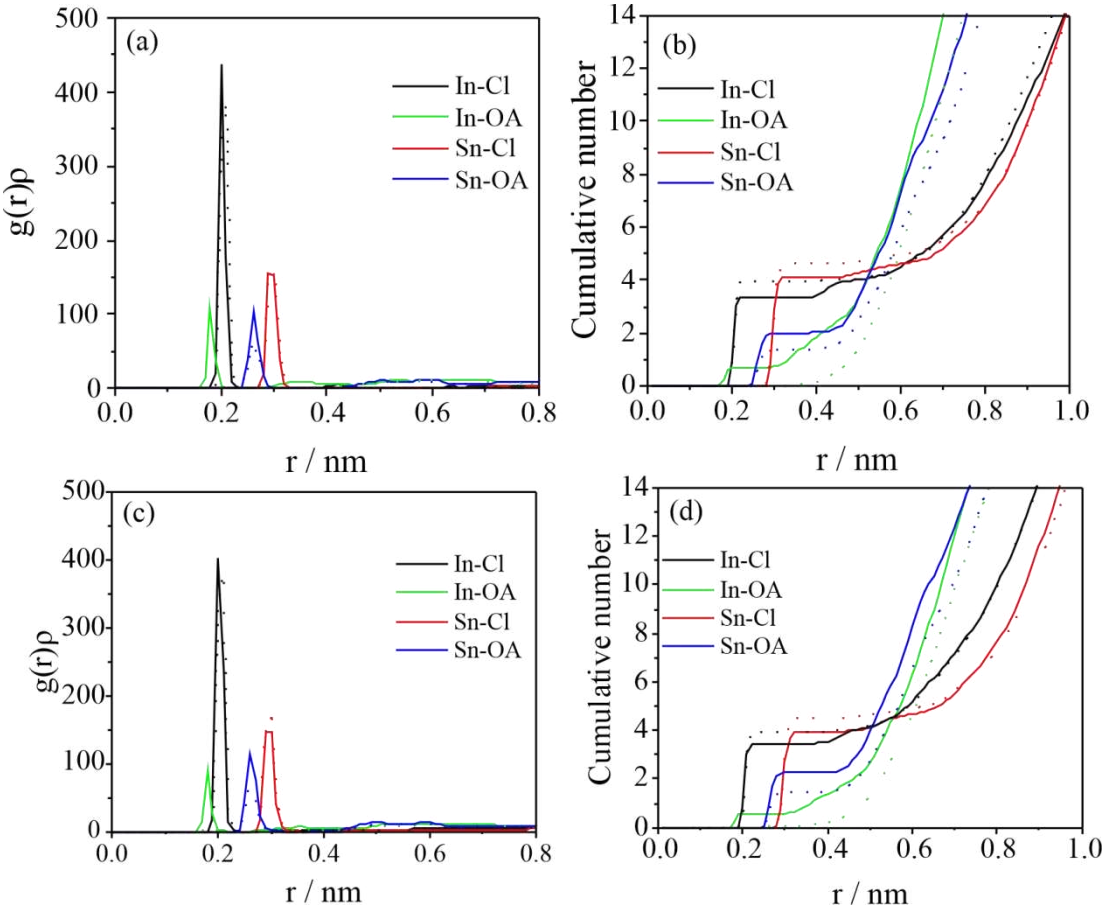

Fig. 1 (a) Radial distribution function multiplied by the average number density [g(r)ρ] for the $Sn^{2+}In^{3+}$ 1:1 system. (b) Cumulative Coordination Number (CCN) for the $Sn^{2+}In^{3+}$ 1:1 system. (c) Radial distribution function multiplied by the average number density [g(r)ρ] for the $Sn^{2+}In^{3+}$ 1:4 system. (d) Cumulative Coordination Number (CCN) for the $Sn^{2+}In^{3+}$ 1:4 system. The solid line represents the interactions at 297 K, while the dotted line represents the interactions at 343 K.

It was found, according to the RDF, that the density of ethylene glycol (EG) molecules, denoted by OA, around In^{3+} was significantly reduced at a higher temperature (343 K), indicating the complete breakdown of any interactions between In^{3+} and the oxygen in ethylene glycol. This suggests that the In-OA interaction is less stable. The density of Cl^- ions around Sn^{2+} remained approximately the same.

The Cumulative Coordination Number (CCN) describes the average cumulative amount of counter-species at a given distance from the reference species and is the result of integrating the expression of g(r)ρ [6]. The CCN results in Fig. 1b show that, at a temperature of 297 K, there are, on average, 3.3 chloride ions and 0.7 molecules of ethylene glycol around In^{3+}, while there are, on average, 4.1 chloride ions and 2.0 molecules of ethylene glycol

around Sn^{2+}. At 343 K, there are, on average, 4.0 chloride ions and no ethylene glycol molecules around In^{3+}, while there are, on average, 4.6 chloride ions and 1.4 ethylene glycol molecules around Sn^{2+}.

According to the CCN presented in Fig. 1b, the increase in temperature resulted in an increase in the average amount of Cl^- around In^{3+} (from 2.0 to 4.0 Å) and Sn^{2+} (from 3.0 to 4.3 Å), and a reduction in OA around In^{3+} and Sn^{2+}. As the increase in temperature results in an increase in the kinetic energy of the system as a whole, the interactions between the reference ions and the OA decrease, since this is an ion-dipole interaction, which tends to be weaker than an ion-ion interaction, this being the case with the interactions of the reference ions with the chloride anion. This indicates that reducing the average amount of OA interacting with In^{3+} and Sn^{2+} results in greater availability of these ions in the system, resulting in OA being replaced by Cl^-. Interactions with choline were disregarded in this study because they are negligible, as found by [6].

For the $Sn^{2+}In^{3+}$ 1:4 system, as shown in Fig. 1c, the following sequence of interactions, in descending order, at 297 K: In-Cl > Sn-Cl > Sn-OA > In-OA, where the counter-species are at a distance of approximately 2.0 Å, 3.0 Å, 1.8 Å, and 2.3 Å, respectively, thus following the same trend observed in the $Sn^{2+}In^{3+}$ 1:1 system. The phenomenology relating to the differences in the magnitude of the densities of counter-species interacting with the reference species is associated with the charges and ionic radius of Sn^{2+} and In^{3+}, similar to the $Sn^{2+}In^{3+}$ 1:1 system.

The CCN results presented in Fig.1d show that, at 297 K, there are, on average, 3.4 chloride ions and 0.6 ethylene glycol molecules around In^{3+}, while there are, on average, 3.9 chloride ions and 2.3 ethylene glycol molecules around Sn^{2+}. At 343 K, there are, on average, 4.0 chloride ions and no ethylene glycol molecules around In^{3+}, while there are, on average, 4.5 chloride ions and 1.5 ethylene glycol molecules around Sn^{2+}. The average amounts of counter-species for each temperature are close to the $Sn^{2+}In^{3+}$ 1:1 system. In addition, it was observed that the average quantity of chloride ions increased around the reference species, and the opposite in relation to the ethylene glycol molecules, the explanation for which is also associated with the stability of the interactions, as discussed in the $Sn^{2+}In^{3+}$ 1:1 system.

In relation to topological information, the Electron Density [ρ(r)] is used to quantify the strength of the interactions [29] between different species in the system studied, as well as the Electron Localization Function (ELF, η) [6]. In addition, the Laplacian of the Electron

Density ($\nabla^2\rho$) describes the nature of an interaction. If the Laplacian is positive, this indicates that the electron density at a given critical bond point is small, suggesting that the density is located in the attractors, characterizing intermolecular interactions [28]. The data related to the topological analysis are presented in tables 2 and 3 and figures 2 and 3.

Table 2 Topological data of In^{3+} and Sn^{2+} ions in the Sn^{2+}:In^{3+} 1:1 (297 K) and Sn^{2+}:In^{3+} 1:1 (343 K) systems. The ELF value, η(r), electron density, ρ(r), and Laplacian of electron density, $\nabla^2\rho(r)$, of the In-Cl, In-OA, Sn-Cl and Sn-OA interactions are presented.

	Sn^{2+}:In^{3+} 1:1 (297 K)				**Sn^{2+}:In^{3+} 1:1 (343 K)**		
	In-Cl	In-OA	Sn-Cl	Sn-OA	In-Cl	Sn-Cl	Sn-OA
Σρ(r)	4.80×10^{-1}	1.31×10^{-1}	1.04×10^{-1}	5.13×10^{-2}	5.69×10^{-1}	1.06×10^{-1}	2.50×10^{-2}
$\Sigma\nabla^2\rho(r)$	1.76	7.73×10^{-1}	2.33×10^{-1}	1.46×10^{-1}	2.13	2.51×10^{-1}	6.43×10^{-2}
Ση(r)	2.62	7.89×10^{-1}	8.73×10^{-1}	2.65×10^{-1}	3.44	8.29×10^{-1}	1.58×10^{-1}

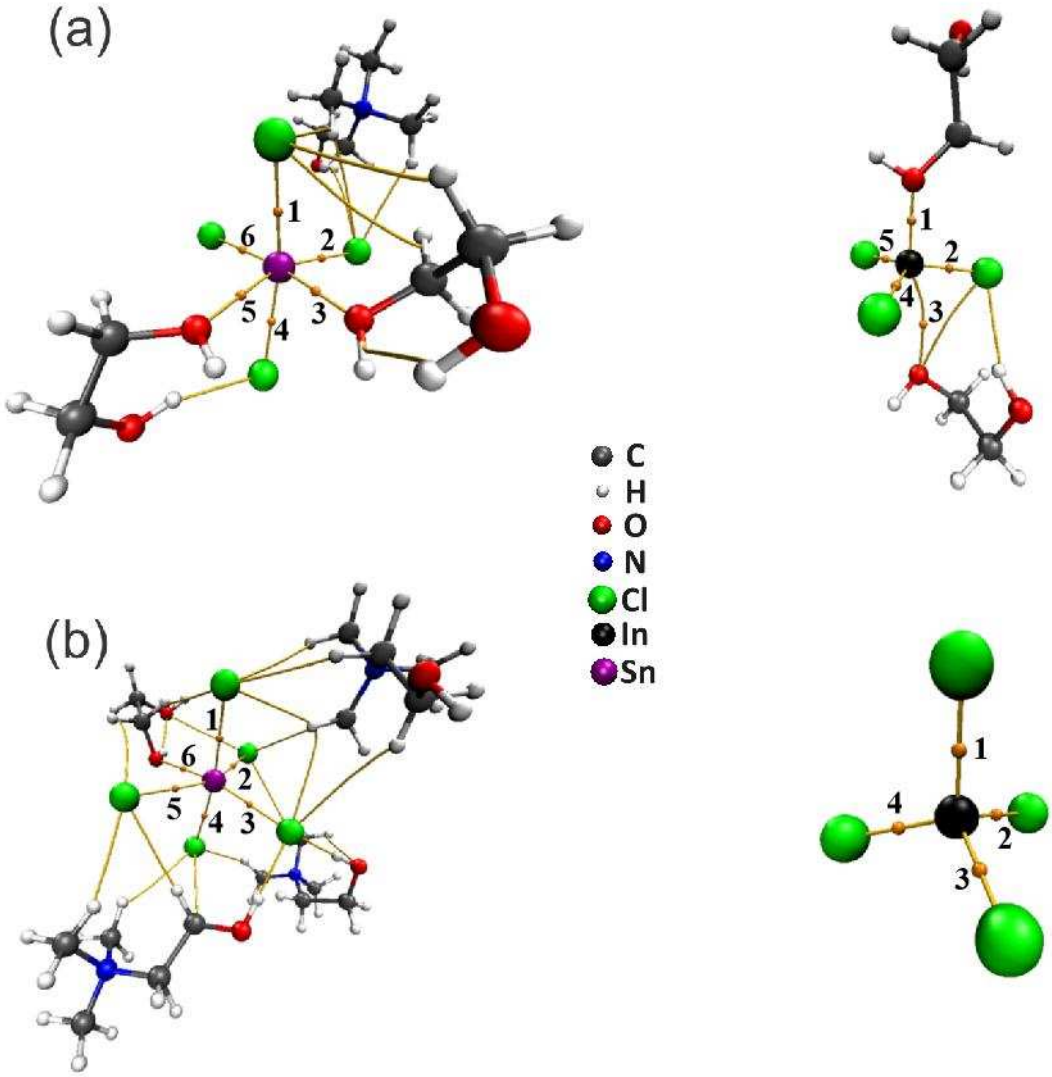

Fig. 2 Molecular graphs with BCPs of Sn^{2+} and In^{3+} in the system (a) Sn^{2+}:In^{3+} 1:1 (297 K) and (b) Sn^{2+}:In^{3+} 1:1 (343 K). Indium (black); Tin (purple); Chloride (green); Carbon (gray); Hydrogen (white); Oxygen (red); Nitrogen (blue).

Table 3 Topological data of In^{3+} and Sn^{2+} ions in the Sn^{2+}:In^{3+} 1:4 (297 K) and Sn^{2+}:In^{3+} 1:4 (343 K) systems. The ELF value, η(r), electron density, ρ(r), and Laplacian of electron density, $\nabla^2\rho(r)$, of the In-Cl, In-OA, Sn-Cl and Sn-OA interactions are presented.

	Sn^{2+}:In^{3+} 1:4 (297 K)				**Sn^{2+}:In^{3+} 1:4 (343 K)**		
	In-Cl	In-OA	Sn-Cl	Sn-OA	In-Cl	Sn-Cl	Sn-OA
Σρ(r)	4.70×10^{-1}	1.36×10^{-1}	1.02×10^{-1}	5.99×10^{-2}	5.33×10^{-1}	1.22×10^{-1}	2.38×10^{-2}
$\Sigma\nabla^2\rho(r)$	1.72	8.35×10^{-1}	2.29×10^{-1}	1.72×10^{-1}	1.99	2.87×10^{-1}	6.78×10^{-2}
Ση(r)	2.61	7.96×10^{-1}	8.44×10^{-1}	3.20×10^{-1}	3.43	9.81×10^{-1}	1.16×10^{-1}

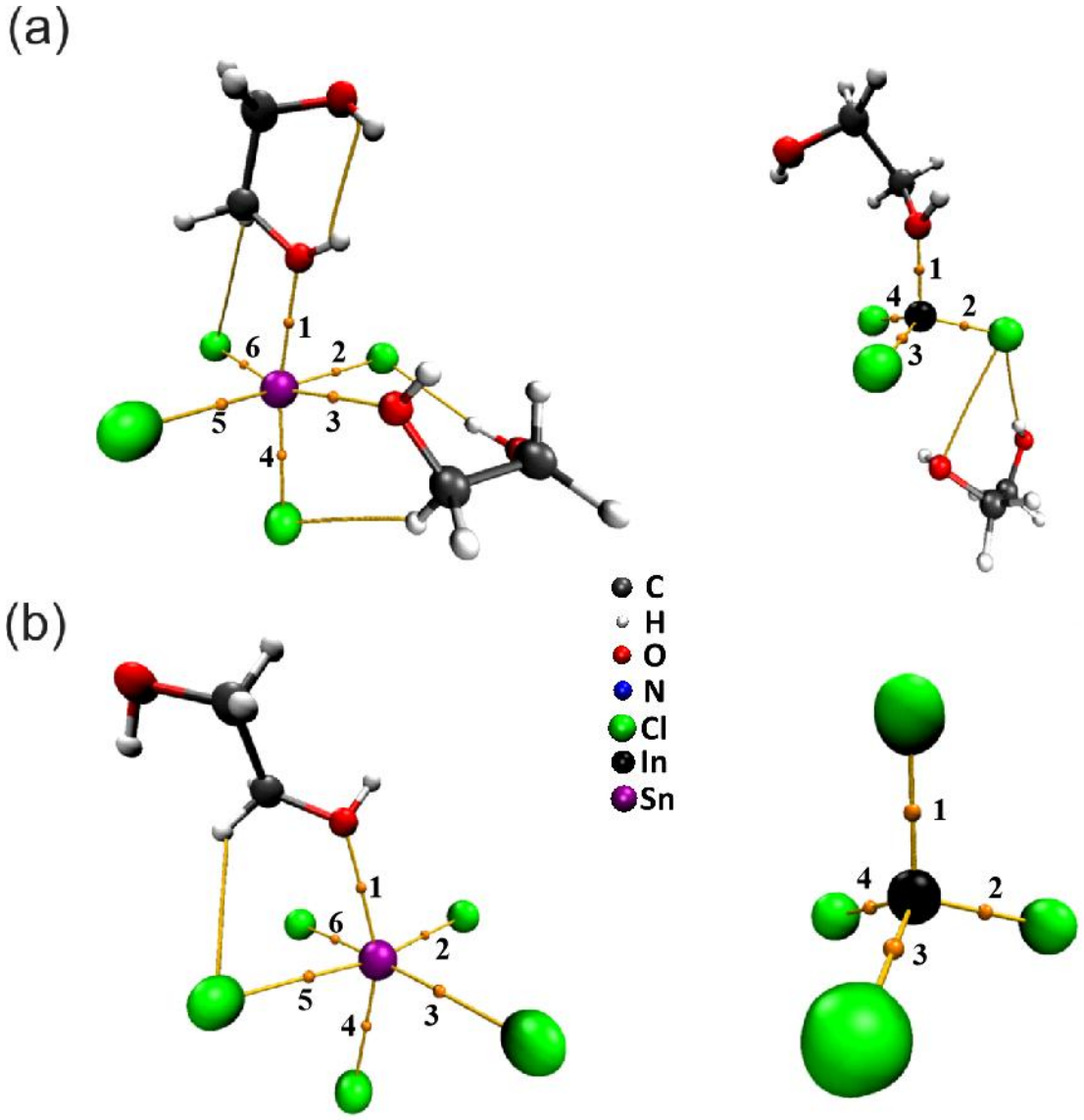

Fig. 3 Molecular graphs with BCPs of Sn^{2+} and In^{3+} in the system (a) Sn^{2+}:In^{3+} 1:4 (297 K) and (b) Sn^{2+}:In^{3+} 1:4 (343 K). Indium (black); Tin (purple); Chloride (green); Carbon (gray); Hydrogen (white); Oxygen (red).

In the molecular graphs presented, it was found that the interaction of the Sn^{2+} ion with the counter-species forms a complex with an approximately octahedral geometry, while the interaction of the complexing species with the In^{3+} ion forms a tetrahedral geometry in the Sn^{2+}:In^{3+} 1:1 (343 K), Sn^{2+}:In^{3+} 1:4 (297 K), and Sn^{2+}:In^{3+} 1:4 (343 K) systems, and a trigonal bipyramidal geometry in the system Sn^{2+}:In^{3+} 1:1 (297 K). The Bond Critical Points (BCPs) where the topological properties [$\rho(r), \nabla^2\rho$ and η] were obtained, were represented by orange spheres located between the reference species and the counter-species.

The Sn-In pairs were selected so that they were consistent with the average values observed in the CCN graphs and with the quantitative differences observed with increasing temperature. Thus, in the systems simulated at 297 K, systems were selected in which there are four chloride ions and two ethylene glycol molecules complexing Sn^{2+}, and three chloride ions and one ethylene glycol molecule complexing In^{3+}. For the systems simulated at 343 K, we selected the systems in which there are five chloride ions and one ethylene glycol molecule complexing Sn^{2+}, and four chloride ions complexing In^{3+}. In the Sn^{2+}:In^{3+} 1:1 (297 K) system, in particular, we observed the formation of bonding paths between In^{3+} and two molecules of ethylene glycol; however, the interaction between In^{3+} and the ethylene glycol underneath has a lower electron density [ρ(r)] and is not a significant part of the sum of the electron density of the In-OA interaction.

It can be seen that for all the systems analyzed in the absence of any surfactants [Sn^{2+}:In^{3+} 1:1 (297 K), Sn^{2+}:In^{3+} 1:1 (343 K), Sn^{2+}:In^{3+} 1:4 (297 K), and Sn^{2+}:In^{3+} 1:4 (343 K)], the electron density of the In-Cl interaction is consistently higher, indicating that this interaction is stronger or more polarized. On the other hand, the Sn-OA interaction showed the lowest electron density in all cases, suggesting that this interaction is the weakest or most diffuse. The same trend was observed by [7] when analyzing the interactions of metal cations with Cl^- and OA.

According to the results, positive $\nabla^2\rho(r)$ values were obtained for all the interactions, indicating their intermolecular nature. The In-Cl interaction has the highest $\nabla^2\rho(r)$ value for all the systems analyzed, and therefore has the highest electron density depletion.

A higher numerical value of ELF implies greater electron confinement in a given region and is strongly related to electron density. In this way, the measurement of ELF is also related to the strength of the interactions [48], and a similar trend to that of electron density is observed.

In all systems without surfactants, the differences observed, in terms of the magnitude of the numerical values, are not pronounceable. With the exception of the exact value of each property, the trends are predominantly the same.

5.2. $Sn^{2+}In^{3+}$ 1:1 + CTAB and $Sn^{2+}In^{3+}$ 1:4 + CTAB

According to the g(r)ρ results, the density of counter-species around the reference ions follows the same trend observed in the systems without surfactants with a Sn:In ratio of 1:4. Bearing in mind that only a single unit of the surfactant CTAB was inserted into the systems

(a quantity representative of the experimental concentration) and that it is a cationic surfactant, no significant interactions were observed between the CTA^+ cation and the reference ions (In-N1 and Sn-N1 interactions). The CCN results show that, in the same way as the systems already presented, increasing the temperature leads to the replacement of ethylene glycol molecules by chloride ions, around In^{3+} and Sn^{2+}. The g(r)ρ and CCN results in question are shown in Fig. 4.

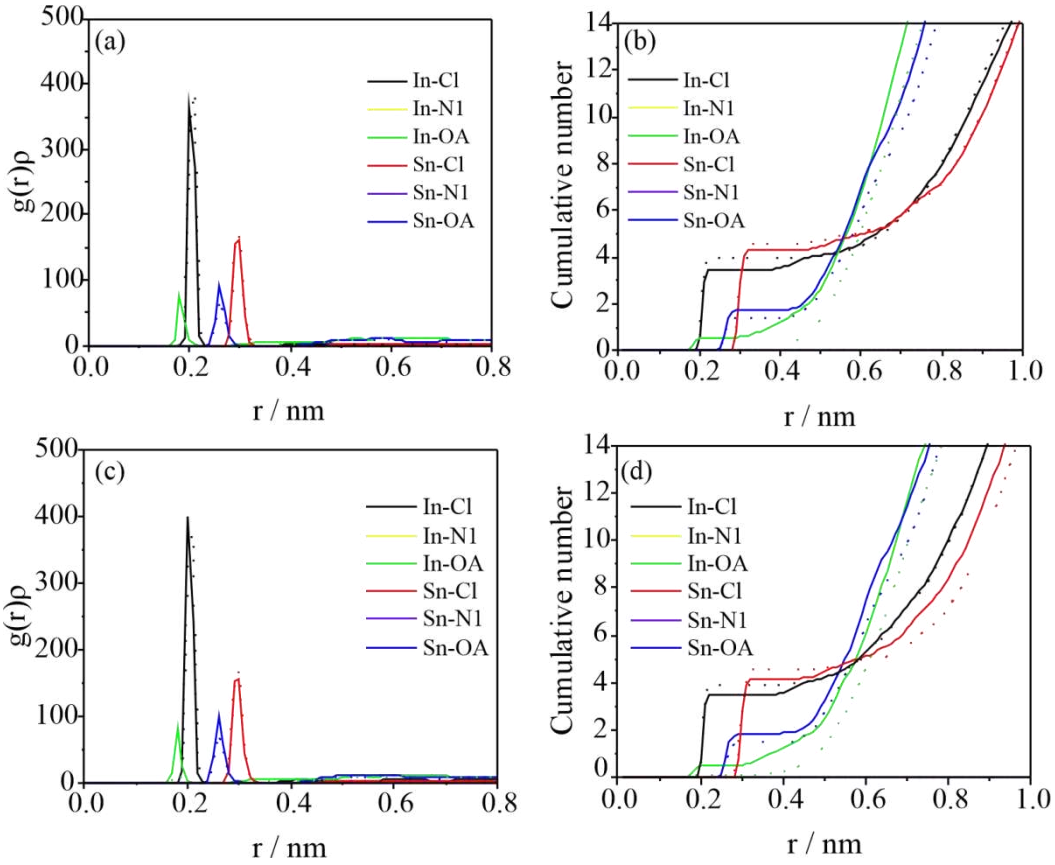

Fig. 4 (a) Radial distribution function multiplied by the average number density [g(r)ρ] for the $Sn^{2+}In^{3+}$ 1:1 + CTAB system. (b) Cumulative Coordination Number (CCN) for the $Sn^{2+}In^{3+}$ 1:1 + CTAB system. (c) Radial distribution function multiplied by the average number density [g(r)ρ] for the $Sn^{2+}In^{3+}$ 1:4 + CTAB system. (d) Cumulative Coordination Number (CCN) for the $Sn^{2+}In^{3+}$ 1:4 + CTAB system. The solid line represents the interactions at 297 K, while the dotted line represents the interactions at 343 K.

Although the surfactant in question does not establish a direct interaction with any of the reference species, there is still a slight reduction in the magnitude of some specific interactions, such as In-Cl. In solution, CTA^+ will not interact exclusively with the bromide ion, Br^-, a component of the CTAB surfactant, but also with chloride ions, which contributes

to a reduction in the density of Cl^- around In^{3+}. The data related to the topological analysis are presented in tables 4 and 5 and figures 5 and 6.

Table 4 Topological data of In^{3+} and Sn^{2+} ions in the Sn^{2+}:In^{3+} 1:1 + CTAB (297 K) and Sn^{2+}:In^{3+} 1:1 + CTAB (343 K) systems. The ELF value, η(r), electron density, ρ(r), and Laplacian of electron density, $\nabla^2\rho(r)$, of the In-Cl, In-OA, Sn-Cl and Sn-OA interactions are presented.

	Sn^{2+}:In^{3+} 1:1 + CTAB (297 K)				**Sn^{2+}:In^{3+} 1:1 + CTAB (343 K)**		
	In-Cl	In-OA	Sn-Cl	Sn-OA	In-Cl	Sn-Cl	Sn-OA
$\Sigma\rho(r)$	4.50×10^{-1}	1.62×10^{-1}	1.09×10^{-1}	5.78×10^{-2}	5.58×10^{-1}	1.24×10^{-1}	2.90×10^{-2}
$\Sigma\nabla^2\rho(r)$	1.65	9.83×10^{-1}	2.45×10^{-1}	1.67×10^{-1}	2.08	2.95×10^{-1}	8.46×10^{-2}
$\Sigma\eta(r)$	2.61	8.26×10^{-1}	8.95×10^{-1}	3.00×10^{-1}	3.44	9.48×10^{-1}	1.52×10^{-1}

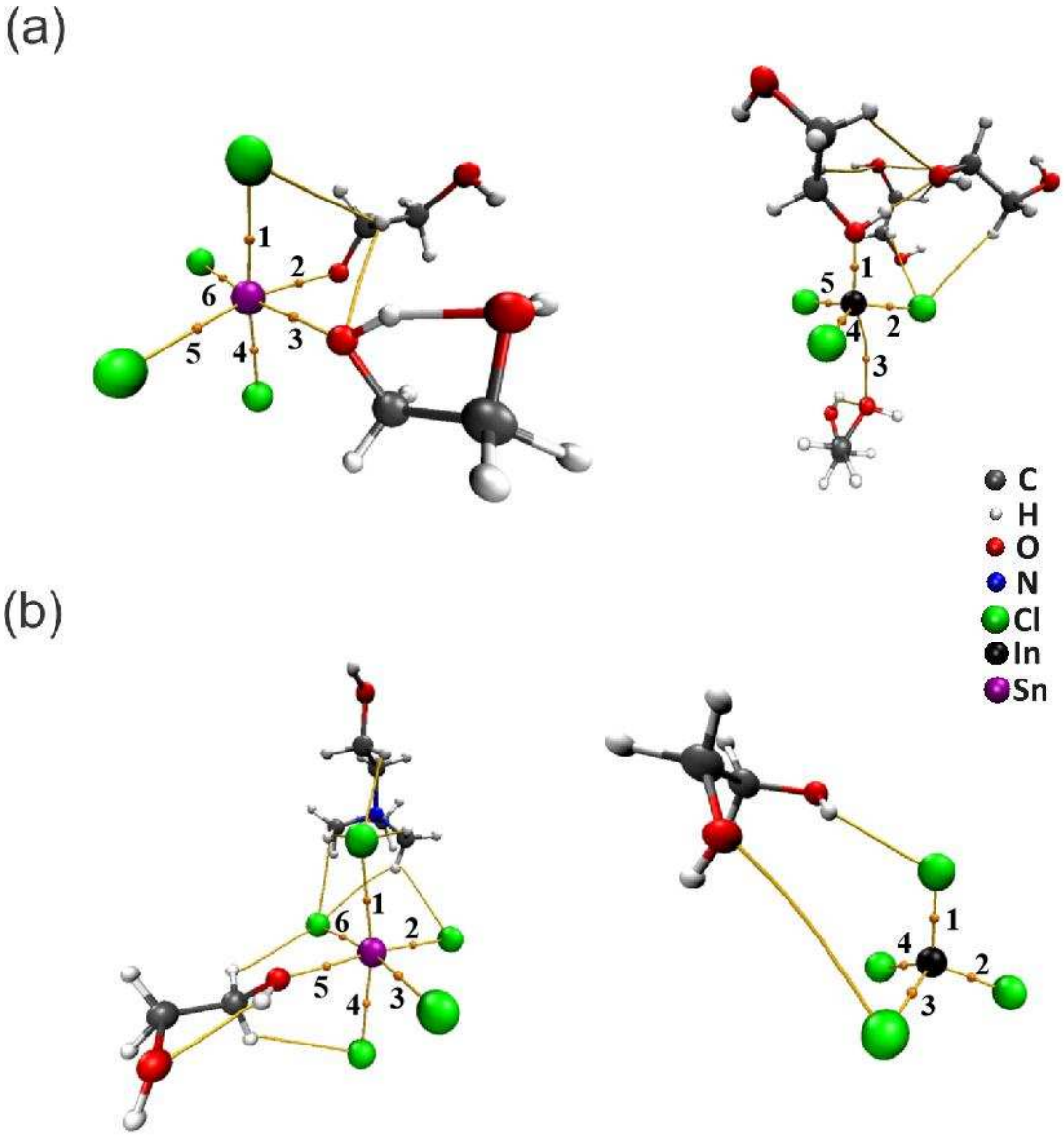

Fig. 5 Molecular graphs with BCPs of Sn^{2+} and In^{3+} in the system (a) Sn^{2+}:In^{3+} 1:1 + CTAB (297 K) and (b) Sn^{2+}:In^{3+} 1:1 + CTAB (343 K). Indium (black); Tin (purple); Chloride (green); Carbon (gray); Hydrogen (white); Oxygen (red); Nitrogen (blue).

Table 5 Topological data of In^{3+} and Sn^{2+} ions in the Sn^{2+}:In^{3+} 1:4 + CTAB (297 K) and Sn^{2+}:In^{3+} 1:4 + CTAB (343 K) systems. The ELF value, η(r), electron density, ρ(r), and Laplacian of electron density, $\nabla^2\rho(r)$, of the In-Cl, In-OA, Sn-Cl and Sn-OA interactions are presented.

	Sn^{2+}:In^{3+} 1:4 + CTAB (297 K)				**Sn^{2+}:In^{3+} 1:4 + CTAB (343 K)**		
	In-Cl	In-OA	Sn-Cl	Sn-OA	In-Cl	Sn-Cl	Sn-OA
Σρ(r)	4.86×10^{-1}	1.32×10^{-1}	1.07×10^{-1}	6.15×10^{-2}	5.65×10^{-1}	1.25×10^{-1}	2.85×10^{-2}

$\Sigma\nabla^2\rho(r)$	1.76	7.81×10^{-1}	2.44×10^{-1}	1.82×10^{-1}	2.12	2.94×10^{-1}	8.63×10^{-2}
$\Sigma\eta(r)$	2.62	7.98×10^{-1}	8.66×10^{-1}	3.22×10^{-1}	3.45	9.55×10^{-1}	1.39×10^{-1}

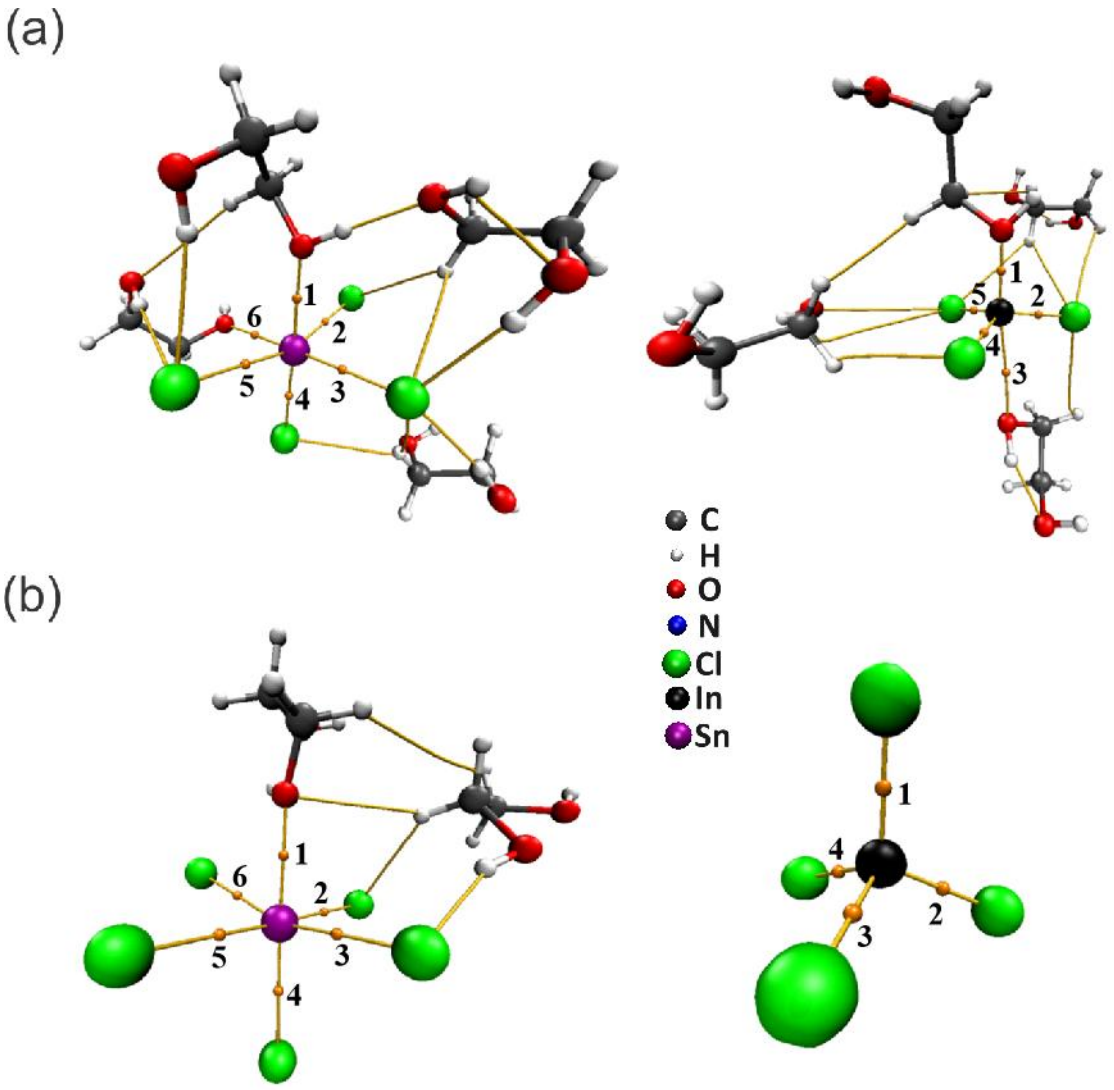

Fig. 6 Molecular graphs with BCPs of Sn^{2+} and In^{3+} in the system (a) Sn^{2+}:In^{3+} 1:4 + CTAB (297 K) and (b) Sn^{2+}:In^{3+} 1:4 + CTAB (343 K). Indium (black); Tin (purple); Chloride (green); Carbon (gray); Hydrogen (white); Oxygen (red).

It was observed that, in the systems with the CTAB surfactant, the geometric structure of the complexes formed is, similarly to what was observed in the systems without surfactants, octahedral for Sn^{2+}, tetrahedral for In^{3+} in the Sn^{2+}:In^{3+} 1:1 + CTAB (343 K) and Sn^{2+}:In^{3+} 1:4 + CTAB (343 K) systems, and trigonal bipyramidal in the Sn^{2+}:In^{3+} 1:1 + CTAB (297 K) and Sn^{2+}:In^{3+} 1:4 + CTAB (297 K) systems. These graphs were obtained in such a way as to be representative of the average values observed in the CCN graphs, so the addition of the

surfactant CTAB in the quantity it was added did not lead to changes in the geometry of the complexes formed.

The ρ(r) and ELF values for all the systems are consistent with the values observed for the systems without surfactants. The In^{3+} interactions with Cl^{-} showed greater strength or polarization. The Laplacian values of the electron density were again positive, indicating that the interactions of the reference species with the counter-species are predominantly intermolecular.

The differences observed in the values of ρ(r), $\nabla^2\rho(r)$ and η(r) in the systems with and without CTAB are subtle and do not necessarily indicate a change in the strength and nature of the interactions. The presence of CTAB can influence the interactions in a subtle way, but this influence is not discernible by the topological analysis since this is an analysis of a single sample of the Sn-In pair that makes up the system.

5.3. $Sn^{2+}In^{3+}$ 1:1 + SDS and $Sn^{2+}In^{3+}$ 1:4 + SDS

It can be seen from the g(r)ρ results that, like the other systems already presented, the density of counter-species around the reference species follows roughly the same trend. However, this time, there was reasonably significant interference from the anionic surfactant SDS, whose interactions were denoted as In-OC and Sn-OC (OC = oxygen of the DS^{-} ion), as shown in Fig. 7.

In the system simulated at 297 K, with a Sn:In ratio of 1:1, the surfactant interferes through the interaction of DS^{-} with In^{3+}, which did not occur with Sn^{2+}. This is due to the amount of SDS that was inserted into the system, which, although greater than that of CTAB in the systems in which this surfactant was inserted, is still not enough to lead to significant interactions with both reference species. Furthermore, the interaction with In^{3+}, specifically, is due to the trivalent nature of this ion, giving it greater interaction with any anions present in the system, including DS^{-}.

However, in the system simulated at a Sn:In ratio of 1:4, the interaction of DS^{-} with In^{3+} was not observed. Furthermore, there was an increase in the magnitude of the density of Cl^{-} ions interacting with In^{3+}. This can be explained by the increase in the amount of chloride ions, which is sufficient to neutralize the inserted In^{3+} ions, while the amount of surfactant is kept constant. The In-Cl interaction is more stable than In-OC, since in the DS^{-} anion, the total negative charge is distributed along the ion chain, resulting in a lower concentration of

charge on the interacting oxygen atoms, unlike the Cl^- anion, in which the total charge is exclusively concentrated on the chlorine.

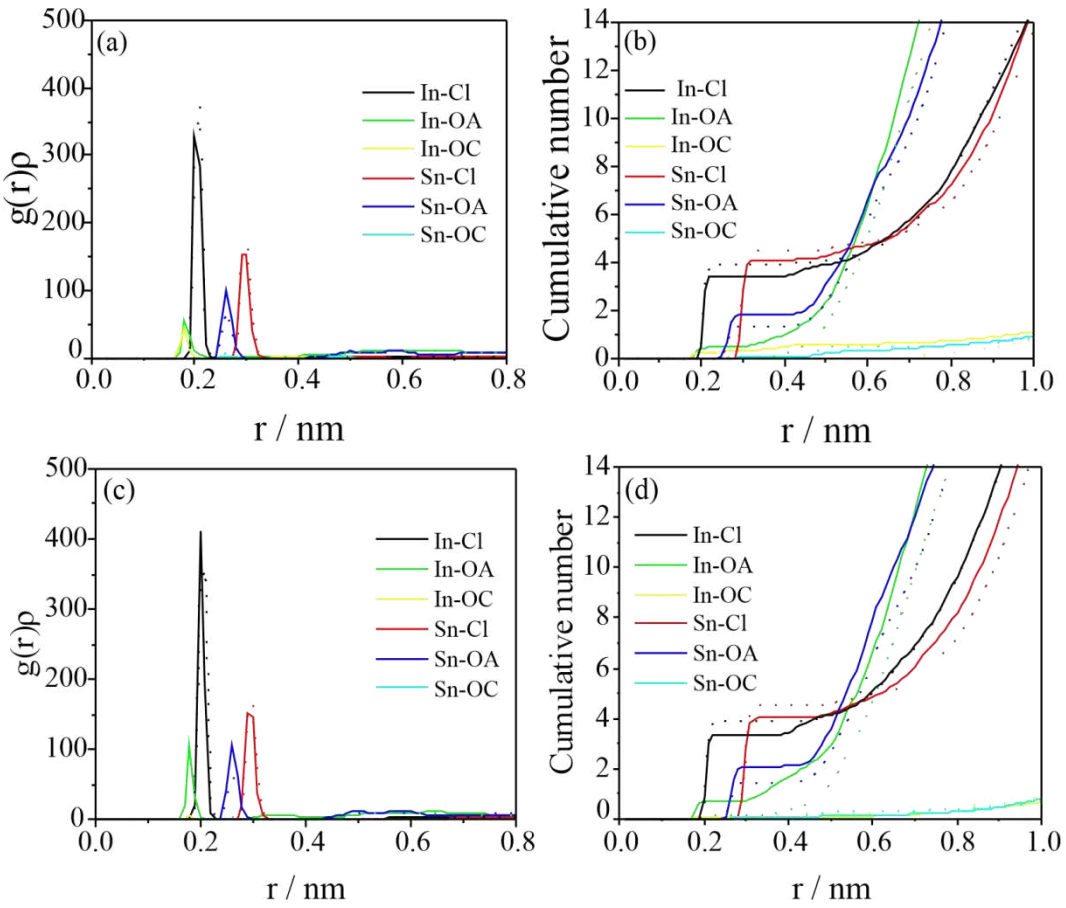

Fig. 7 (a) Radial distribution function multiplied by the average number density [g(r)ρ] for the $Sn^{2+}In^{3+}$ 1:1 + SDS system. (b) Cumulative Coordination Number (CCN) for the $Sn^{2+}In^{3+}$ 1:1 + SDS system. (c) Radial distribution function multiplied by the average number density [g(r)ρ] for the $Sn^{2+}In^{3+}$ 1:4 + SDS system. (d) Cumulative Coordination Number (CCN) for the $Sn^{2+}In^{3+}$ 1:4 + SDS system. The solid line represents the interactions at 297 K, while the dotted line represents the interactions at 343 K.

The CCN graphs show that the system has approximately the same behavior observed in the systems with added CTAB as well as in the systems without additives for the In-Cl, In-OA, Sn-Cl and Sn-OA interactions. However, in the Sn^{2+}:In^{3+} 1:1 (297 K) system, a slight amount of DS^- (0.3 on average) was observed interacting with In^{3+}, consistent with what is indicated by g(r)ρ. The data related to the topological analysis are presented in tables 6 and 7 and figures 8 and 9.

Table 6 Topological data of In^{3+} and Sn^{2+} ions in the Sn^{2+}:In^{3+} 1:1 + SDS (297 K) and Sn^{2+}:In^{3+} 1:1 + SDS (343 K) systems. The ELF value, η(r), electron density, ρ(r), and Laplacian of electron density, $\nabla^2\rho(r)$, of the In-Cl, In-OA, Sn-Cl and Sn-OA interactions are presented.

	Sn^{2+}:In^{3+} 1:1 + SDS (297 K)				**Sn^{2+}:In^{3+} 1:1 + SDS (343 K)**		
	In-Cl	In-OA	Sn-Cl	Sn-OA	In-Cl	Sn-Cl	Sn-OA
Σρ(r)	4.84×10^{-1}	1.49×10^{-1}	1.01×10^{-1}	5.23×10^{-2}	5.62×10^{-1}	1.16×10^{-1}	2.28×10^{-2}
$\Sigma\nabla^2\rho(r)$	1.75	8.75×10^{-1}	2.31×10^{-1}	1.44×10^{-1}	2.10	2.69×10^{-1}	6.10×10^{-2}
Ση(r)	2.62	8.50×10^{-1}	8.21×10^{-1}	2.85×10^{-1}	3.44	9.39×10^{-1}	1.17×10^{-1}

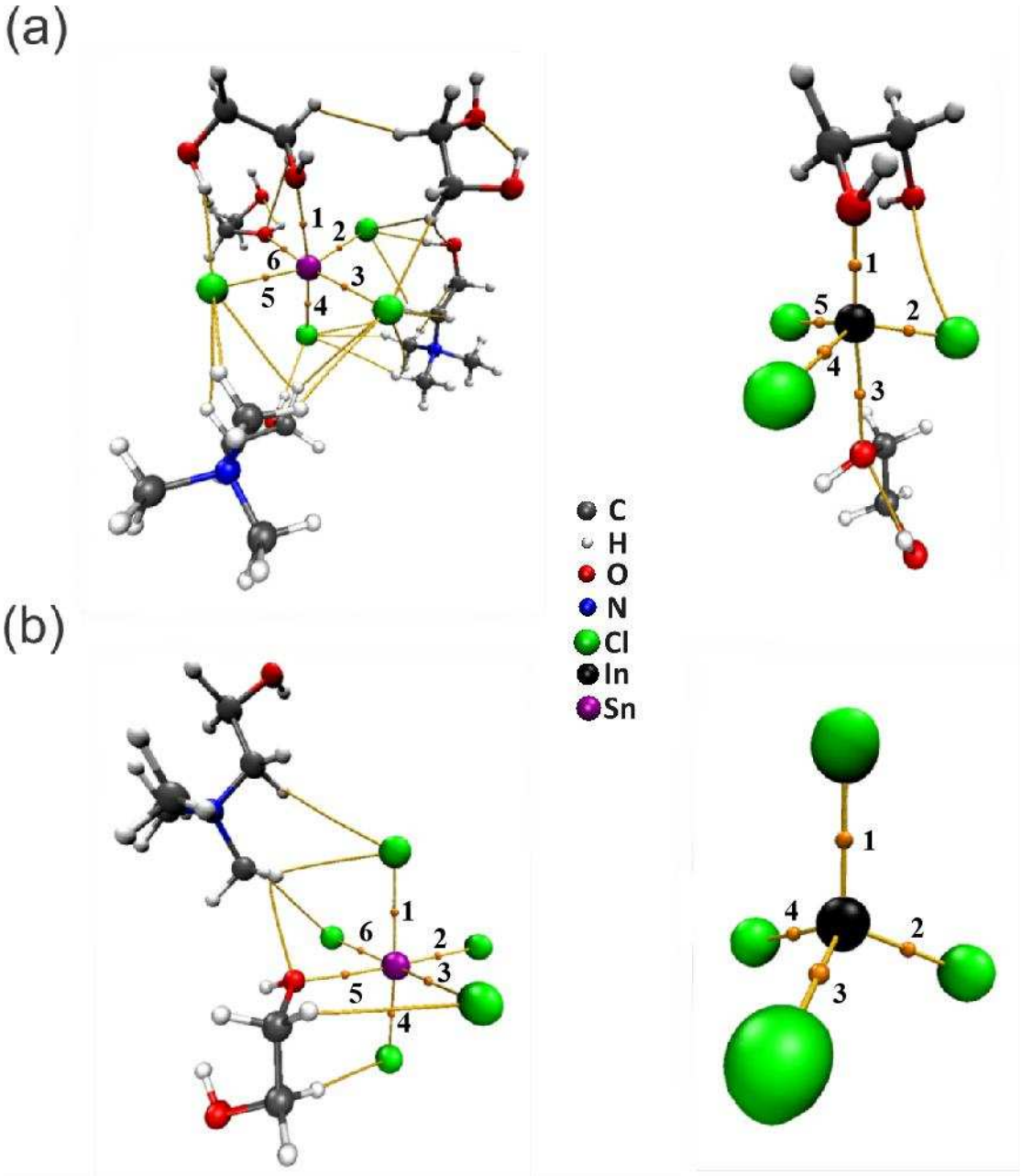

Fig. 8 Molecular graphs with BCPs of Sn^{2+} and In^{3+} in the system (a) Sn^{2+}:In^{3+} 1:1 + SDS (297 K) and (b) Sn^{2+}:In^{3+} 1:1 + SDS (343 K). Indium (black); Tin (purple); Chloride (green); Carbon (gray); Hydrogen (white); Oxygen (red); Nitrogen (blue).

Table 7 Topological data of In^{3+} and Sn^{2+} ions in the Sn^{2+}:In^{3+} 1:4 + SDS (297 K) and Sn^{2+}:In^{3+} 1:4 + CTAB (343 K) systems. The ELF value, η(r), electron density, ρ(r), and Laplacian of electron density, $\nabla^2\rho(r)$, of the In-Cl, In-OA, Sn-Cl and Sn-OA interactions are presented.

	Sn^{2+}:In^{3+} 1:4 + SDS (297 K)				**Sn^{2+}:In^{3+} 1:4 + SDS (343 K)**		
	In-Cl	In-OA	Sn-Cl	Sn-OA	In-Cl	Sn-Cl	Sn-OA

$\Sigma\rho(r)$	4.70×10^{-1}	1.62×10^{-1}	9.74×10^{-2}	5.94×10^{-2}	5.69×10^{-1}	1.27×10^{-1}	2.74×10^{-2}
$\Sigma\nabla^2\rho(r)$	1.74	9.89×10^{-1}	2.21×10^{-1}	1.78×10^{-1}	2.12	3.01×10^{-1}	7.88×10^{-2}
$\Sigma\eta(r)$	2.61	8.15×10^{-1}	8.05×10^{-1}	3.06×10^{-1}	3.44	9.68×10^{-1}	1.46×10^{-1}

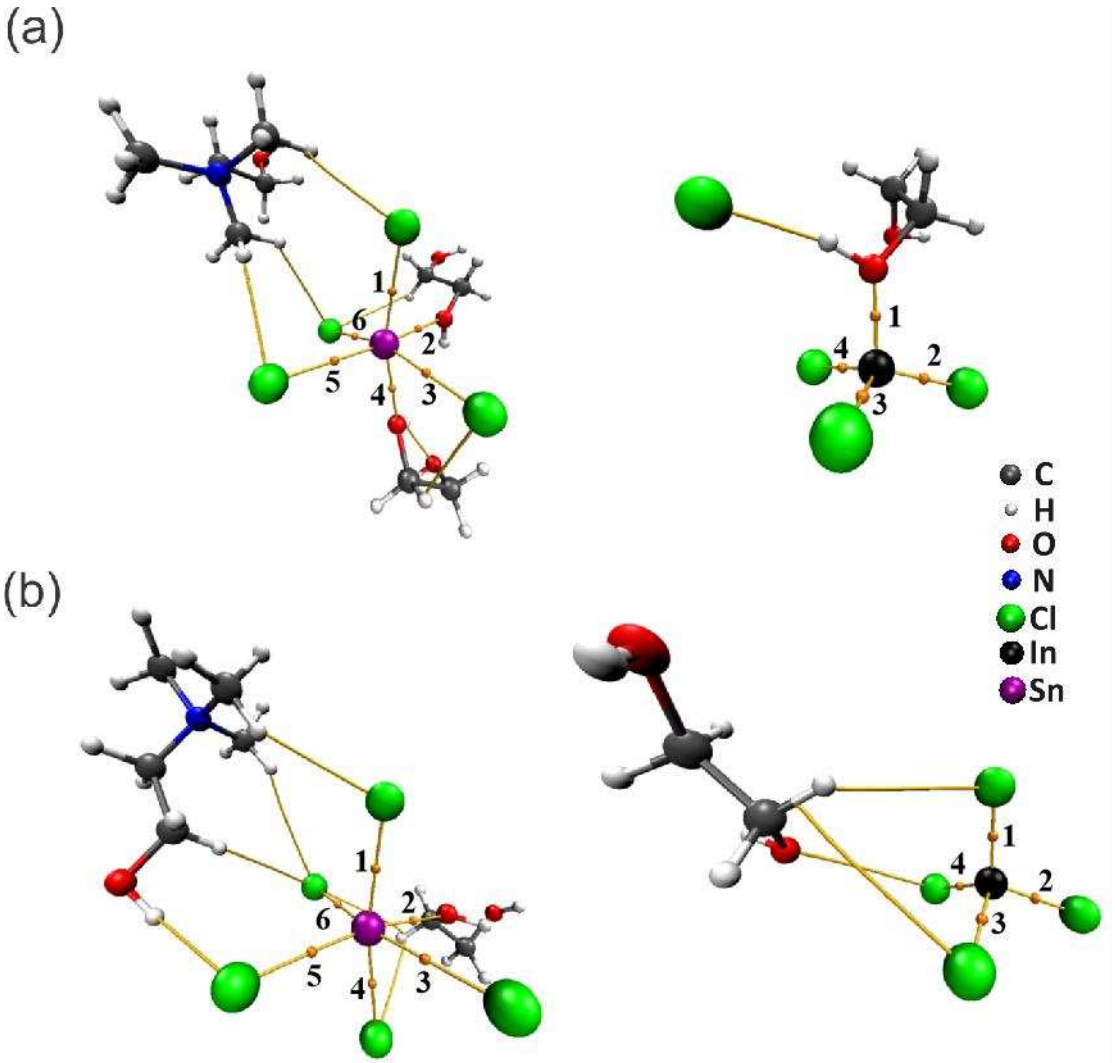

Fig. 9 Molecular graphs with BCPs of Sn^{2+} and In^{3+} in the system (a) Sn^{2+}:In^{3+} 1:4 + SDS (297 K) and (b) Sn^{2+}:In^{3+} 1:4 + SDS (343 K). Indium (black); Tin (purple); Chloride (green); Carbon (gray); Hydrogen (white); Oxygen (red); Nitrogen (blue).

The molecular graphs of the systems with the SDS additive show the geometric structures of the complexes formed around the reference species, which, like the other systems already presented, are octahedral for Sn^{2+}, tetrahedral for In^{3+} in the Sn^{2+}:In^{3+} 1:1 + SDS (343 K), Sn^{2+}:In^{3+} 1:4 + SDS (297 K) and Sn^{2+}:In^{3+} 1:4 + SDS (343 K) systems, and trigonal bipyramidal for the Sn^{2+}:In^{3+} 1:1 + SDS (297 K) system. It is worth noting that

although the choline cation was observed around Sn^{2+}, it does not interact directly with the reference ion in question, as indicated by the bond paths.

In addition, the strength and character of the interactions followed the same trend already observed in the other conditions evaluated, with the In-Cl interaction showing greater strength or polarization and all the interactions showing intermolecular character. There is no clear evidence of the influence of SDS on the topological properties of the system.

6. Conclusions

The Radial Distribution Function multiplied by the Average Numerical Density [g(r)ρ] and the Cumulative Coordination Number (CCN) revealed consistent patterns of interaction between the reference species, In^{3+} and Sn^{2+}, with the counter-species, Cl^{-} and OA (OA = oxygen from ethylene glycol). It was found that In^{3+} tends to interact more strongly with Cl^{-} compared to Sn^{2+}, while the interaction with OA is weaker and less stable, especially at a higher temperature, since, in the system simulated at 343 K, there was an increase in the amount of Cl^{-} around the reference ions and a reduction in the amount of OA. The Electron Density [ρ(r)] and Electron Localization Function (ELF) showed that the In-Cl interactions are stronger or more polarized in all systems. The Laplacian of the Electron Density ($\nabla^2\rho$) was consistently positive, indicating an intermolecular nature on the part of all interactions of counter-species with the reference species. Finally, the insertion of surfactants subtly altered some specific interactions. With CTAB, there was a slight reduction in the magnitude of the In-Cl interaction, while SDS mainly influenced interactions with In^{3+}, as shown by g(r)ρ, based on the trivalent nature of In^{3+} and the anionic nature of SDS.

REFERENCES

[1] TADEUSZ GOREWODA et al. Microstructural Effect Limitations in the Analysis of SnAg, SnBi and SnIn Lead-free Solders by Wavelength Dispersion X-Ray Spectrometry. **Journal of Analytical Chemistry**, v. 75, n. 1, p. 56–62, 26 jan. 2020.

[2] WU, A. T.; CHEN, M.-H.; HUANG, C.-H. Formation of intermetallic compounds in SnAgBiIn solder systems on Cu substrates. **Journal of Alloys and Compounds**, v. 476, n. 1–2, p. 436–440, maio 2009.

[3] HUMPSTON, G.; JACOBSON, D. M. Indium solders. **Advanced Materials & Processes**, v. 163, n. 4, p. 45–47, 2005.

[4] LUKTUKE, A. et al. Influence of Indium addition on microstructural and mechanical behavior of Sn solder alloys: Experiments and first principles calculations. **Acta Materialia**, v. 249, n. March, p. 118853, maio 2023.

[5] ANICAI et al. Electrodeposition of Sn–In Alloys Involving Deep Eutectic Solvents. **Coatings**, v. 9, n. 12, p. 800, 28 nov. 2019.

[6] VERÍSSIMO DE OLIVEIRA, R. et al. Analysis of the behavior of Sn2+ and In3+ ions in DES and in water: A theoretical approach. **Journal of Molecular Liquids**, v. 353, p. 118774, maio 2022.

[7] SOUSA, N. G. et al. Modelling approach applied to SnIn coatings from choline chloride/ethylene glycol deep eutectic solvent. **Journal of Molecular Liquids**, v. 390, n. PA, p. 122973, nov. 2023.

[8] NAMBA, A. M.; SILVA, V. B. DA; SILVA, C. H. T. P. DA. Dinâmica molecular: teoria e aplicações em planejamento de fármacos. **Eclética Química**, v. 33, n. 4, p. 13–24, dez. 2008.

[9] S. M.; CHANDRASEKARA PILLAI, K. Cetyltrimethyl ammonium bromide surfactant-assisted morphological and electrochemical changes in electrochemically prepared nanoclustered iron(III) hexacyanoferrate. **Journal of Electroanalytical Chemistry**, v. 589, n. 1, p. 167–175, abr. 2006.

[10] CHANDRAN, R.; BEHERA, A. K.; MALLIK, A. Composition Tuning of Single Step Electrodeposited CuInSe2 Thin Films Using Sodium Dodecyl Sulfate as Additive. **Journal of Electronic Materials**, v. 48, n. 12, p. 8129–8137, 25 dez. 2019.

[11] SAI JYOTHEENDER, K.; PUNITH KUMAR, M. K.; SRIVASTAVA, C. Influence of surfactant polarity on the evolution of micro-texture, grain boundary constitution and corrosion behavior of electrodeposited Zn coatings. **Surface and Coatings Technology**, v. 423, n. August, p. 127594, out. 2021.

[12] JYOTHEENDER, K. S.; SRIVASTAVA, C. Effect of geometrically necessary dislocations induced strain on the corrosion behavior of Ni coatings with different surfactants. **Materialia**, v. 22, n. March, p. 101431, maio 2022.

[13] CHEN, L. et al. Effect of three types of surfactants on fabrication of Cu-coated graphite powders. **Advanced Powder Technology**, v. 24, n. 1, p. 281–287, jan. 2013.

[14] KONG, C. X.; NURULAKMAL, M. S.; ONG, H. P. Effect of surfactant and particle size on thickness and hardness of nanocomposite coating Sn/Ag for bus duct conductor. **Materials Today: Proceedings**, v. 66, p. 3020–3024, 2022.

[15] SHIMIZU, M.; HIRAHARA, K.; ARAI, S. Morphology control of zinc electrodeposition by surfactant addition for alkaline-based rechargeable batteries. **Physical Chemistry Chemical Physics**, v. 21, n. 13, p. 7045–7052, 2019.

[16] WICKRAMAARACHCHI, K.; SUNDARAM, M. M.; HENRY, D. Surfactant-mediated electrodeposition of a pseudocapacitive manganese dioxide a twofer. **Journal of Energy Storage**, v. 55, n. PA, p. 105403, nov. 2022.

[17] ARIBOU, Z. et al. Effect of polymer additive on structural and morphological properties of Cu-electrodeposition from an acid sulfate electrolyte: Experimental and theoretical studies. **Journal of Electroanalytical Chemistry**, v. 946, n. July, p. 117722, out. 2023.

[18] BADER, R. F. W. A quantum theory of molecular structure and its applications. **Chemical Reviews**, v. 91, n. 5, p. 893–928, 1 jul. 1991.

[19] DEL GALDO, S.; ASCHI, M.; AMADEI, A. In silico characterization of bimolecular electron transfer reactions: The ferrocene–ferrocenium reaction as a test case. **International Journal of Quantum Chemistry**, v. 116, n. 22, p. 1723–1730, 15 nov. 2016.

[20] MACKERELL, A. D. et al. Integration Schemes for Molecular Dynamics. **Critical Reviews in Biochemistry and Molecular Biology**, v. 159, n. 1, p. 256–259, 1998.

[21] DE OLIVEIRA, André Mauricio. **Introdução à modelagem Molecular para Química, Engenharia e Biomédicas: fundamentos e exercícios**. Appris Editora e Livraria Eireli-ME, 2018.

[22] FONSECA, A.; MARINHO, E.; SANTOS, J. **Uma breve introdução à simulação computacional aplicada à química**. [s.l: s.n.].

[23] DE ALWIS, T. CENTRAL DIFFERENCE FORMULA IN NUMERICAL ANALYSIS. **PRIMUS**, v. 2, n. 2, p. 165–172, jan. 1992.

[24] DONKÓ, Z. et al. eduPIC: an introductory particle based code for radio-frequency plasma simulation. **Plasma Sources Science and Technology**, v. 30, n. 9, p. 095017, 1 set. 2021.

[25] KAUROLA, Petri. **Lateral Diffusion Along Curved Lipid Bilayers**. 2019. Dissertação de Mestrado.

[26] SAUNDERS, William Robert; GRANT, James; MÜLLER, Eike Hermann. A domain specific language for performance portable molecular dynamics algorithms. **Computer Physics Communications**, v. 224, p. 119-135, 2018.

[27] YOUNGE, K. et al. A model system for examining the radial distribution function. **American Journal of Physics**, v. 72, n. 9, p. 1247–1250, 1 set. 2004.

[28] OLIVEIRA, B. G.; ARAÚJO, R. C. M. U.; RAMOS, M. N. A topologia molecular QTAIM e a descrição mecânico-quântica de ligações de hidrogênio e ligações de di-hidrogênio. **Química Nova**, v. 33, n. 5, p. 1155–1162, 2010.

[29] LU, T.; CHEN, F. Multiwfn: A multifunctional wavefunction analyzer. **Journal of Computational Chemistry**, v. 33, n. 5, p. 580–592, 15 fev. 2012.

[30] PARR, R. G. Density functional theory of atoms and molecules BT - horizons of quantum chemistry. **Horizons of Quantum Chemistry**, p. 5–15, 1980.

[31] STEPHEN, P. J. et al. Ab Initio Calculation of Vibrational Absorption. **The Journal of Physical Chemistry**, v. 98, n. 45, p. 11623–11627, 1994.

[32] HOHENBERG, P.; KOHN, W. Inhomogeneous Electron Gas. **Physical Review**, v. 136, n. 3B, p. B864–B871, 9 nov. 1964.

[33] BECKE, A. D. Density-functional thermochemistry. III. The role of exact exchange. **The Journal of Chemical Physics**, v. 98, n. 7, p. 5648–5652, 1 abr. 1993.

[34] LEE, C.; YANG, W.; PARR, R. G. Development of the Colle-Salvetti correlation-energy formula into a functional of the electron density. **Physical Review B**, v. 37, n. 2, p. 785–789, 15 jan. 1988.

[35] VOSKO, S. H.; WILK, L.; NUSAIR, M. Accurate spin-dependent electron liquid correlation energies for local spin density calculations: a critical analysis. **Canadian Journal of Physics**, v. 58, n. 8, p. 1200–1211, 1 ago. 1980.

[36] FRISCH, M. J. et al. Gaussian 09, Revis. B. 01, Gaussian. **Inc., Wallingford CT**, p. 1–20, 2009.

[37] GARCÍA, G.; ATILHAN, M.; APARICIO, S. The impact of charges in force field parameterization for molecular dynamics simulations of deep eutectic solvents. **Journal of Molecular Liquids**, v. 211, p. 506–514, nov. 2015.

[38] BERENDSEN, H. J. C.; VAN DER SPOEL, D.; VAN DRUNEN, R. GROMACS: A message-passing parallel molecular dynamics implementation. **Computer Physics Communications**, v. 91, n. 1–3, p. 43–56, set. 1995.

[39] JORGENSEN, W. L.; TIRADO-RIVES, J. The OPLS [optimized potentials for liquid simulations] potential functions for proteins, energy minimizations for crystals of cyclic peptides and crambin. **Journal of the American Chemical Society**, v. 110, n. 6, p. 1657–1666, 1 mar. 1988.

[40] FARAFONOV, V. S.; LEBED, A. V. Developing and Validating a Set of All-Atom Potential Models for Sodium Dodecyl Sulfate. **Journal of Chemical Theory and Computation**, v. 13, n. 6, p. 2742–2750, 13 jun. 2017.

[41] ARFKEN, George B.; WEBER, Hans J.; HARRIS, Frank E. **Mathematical methods for physicists: a comprehensive guide**. Elsevier, 2013.

[42] BERENDSEN, H. J. C. et al. Molecular dynamics with coupling to an external bath. **The Journal of Chemical Physics**, v. 81, n. 8, p. 3684–3690, 15 out. 1984.

[43] PARRINELLO, M.; RAHMAN, A. Polymorphic transitions in single crystals: A new molecular dynamics method. **Journal of Applied Physics**, v. 52, n. 12, p. 7182–7190, 1 dez. 1981.

[44] LI, X. et al. Computer simulations of aqua metal ions for accurate reproduction of hydration free energies and structures. **The Journal of Chemical Physics**, v. 132, n. 10, 14 mar. 2010.

[45] ZHAO, Y.; TRUHLAR, D. G. The M06 suite of density functionals for main group thermochemistry, thermochemical kinetics, noncovalent interactions, excited states, and transition elements: two new functionals and systematic testing of four M06-class functionals and 12 other function. **Theoretical Chemistry Accounts**, v. 120, n. 1–3, p. 215–241, 12 maio 2008.

[46] WADT, W. R.; HAY, P. J. Ab initio effective core potentials for molecular calculations. Potentials for main group elements Na to Bi. **The Journal of Chemical Physics**, v. 82, n. 1, p. 284–298, 1 jan. 1985.

[47] ABRAHAM, M. W. M. et al. GROMACS 2016 Reference Manual. **GROMACS 2016 Reference Manual**, 2018.

[48] BEZERRA, L. L. et al. Electrochemical and theoretical investigation on the behavior of the Co2+ ion in three eutectic solvents. **Journal of Molecular Graphics and Modelling**, v. 112, n. November 2021, p. 108137, maio 2022.

ANNEX A – PAPER'S DRAFT PROOF

Journal of Molecular Structure

Behavior of Tin and Indium in the DES ethaline: Theoretical and Experimental insights

--Manuscript Draft--

Manuscript Number:	MOLSTRUC-D-24-03924
Article Type:	Research Paper
Keywords:	Electrodeposition; Ethaline; Tin; Indium; CTAB; SDS
Corresponding Author:	Norberto Monteiro Universidade Federal do Ceará Fortaleza, BRAZIL
First Author:	José Júnior
Order of Authors:	José Júnior
	Natalia Sousa
	Renato Oliveira
	Lucas Bezerra
	Adriana Correia
	Pedro Neto
	Norberto Monteiro
Abstract:	This work uses computational and experimental methodologies to investigate the behavior of Sn^{2+} and In^{3+} ions in the DES ethaline under different conditions, such as different temperatures, ion ratios, and in the presence and absence of different surfactants, as well as to analyse the morphology of the electrodeposits. Morphology and composition analysis were performed using Scanning Electron Microscopy (SEM) and Energy Dispersive X-ray (EDS). Twelve Molecular Dynamics (MD) simulations were conducted, using the GROMACS software. Additionally, Quantum Theory of Atoms in Molecules (QTAIM) properties were obtained after MD simulations. The results presented that In^{3+} showed stronger affinity for Cl^- than Sn^{2+}, but weaker and less stable interactions with OA (OA = oxygen of ethylene glycol), particularly at higher temperatures. Electron Density and Electron Localization Function analysis indicated that In-Cl interactions are stronger and more polarized than other interactions. The Laplacian of Electron Density suggested an intermolecular nature for all interactions. The surfactant addition altered these interactions slightly, with CTAB reducing the density of Cl^- around In^{3+} and SDS interacting with In^{3+} at 297 K and in a Sn:In proportion of 1:1. SEM images revealed temperature and potential-dependent changes in film morphology, changing from globular to smooth. CTAB and SDS additions led to uniform coating in Sn^{2+}:In^{3+} solutions, with SDS affecting In content, resulting in $Sn_{68}In_{32}$ and $Sn_{33}In_{67}$ coatings at specific conditions for 1:1 and 1:4 solutions, respectively.
Suggested Reviewers:	CARLOS HUITLE carlos.alberto.mh@ufrn.br
	Davi Vieira davi.vieira@ufrn.br
	SIBELE PERGHER sibele.pergher@ufrn.br